Comparative DFT Study of the Spin Trapping of Methyl, Mercapto, Hydroperoxy, Superoxide, and Nitric Oxide Radicals by Various Substituted Cyclic Nitrones

Frederick A. Villamena,*,† Christopher M. Hadad,*,‡ and Jay L. Zweier*,†

Center for Biomedical EPR Spectroscopy and Imaging, the Davis Heart and Lung Research Institute, and the Division of Cardiovascular Medicine, Department of Internal Medicine, College of Medicine, The Ohio State University, Columbus, Ohio 43210, and Department of Chemistry, 100 W. 18th Avenue, The Ohio State University, Columbus, Ohio 43210

Received: October 25, 2004

The thermodynamics of the spin trapping of various cyclic nitrones with biologically relevant radicals such as methyl, mercapto, hydroperoxy, superoxide anion, and nitric oxide was investigated using computational methods. A density functional theory (DFT) approach was employed in this study at the B3LYP/6-31+G(d,p)//B3LYP/6-31G(d) level. The order of increasing favorability for ΔG_{rxn} (kcal/mol) of the radical reaction with various nitrones, in general, follows a trend similar to their respective experimental reduction potentials as well as their experimental second-order rate constants in aqueous solution: NO (14.57) < $O_2^{\bullet-}$ (−7.51) < $^{\bullet}O_2H$ (−13.92) < $^{\bullet}SH$ (−16.55) < $^{\bullet}CH_3$ (−32.17) < $^{\bullet}OH$ (−43.66). The same qualitative trend is predicted upon considering the effect of solvation using the polarizable continuum model (PCM): i.e., NO (14.12) < $O_2^{\bullet-}$ (9.95) < $^{\bullet}O_2H$ (−6.95) < $^{\bullet}SH$ (−13.57) < $^{\bullet}CH_3$ (−32.88) < $^{\bullet}OH$ (−38.91). All radical reactions with these nitrones are exoergic, except for NO (and $O_2^{\bullet-}$ in the aqueous phase), which is endoergic, and the free energy of activation ($\Delta G^{\ddagger}$) for the NO additions ranges from 17.7 to 20.3 kcal/mol. This study also predicts the favorable formation of certain adducts that exhibit intramolecular H-bonding interactions, nucleophilic addition, or H-atom transfer reactions. The spin density on the nitronyl N of the superoxide adducts reveals conformational dependences. The failure of nitrones to trap NO at normal conditions was theoretically rationalized due to the endoergic reaction parameters.

I. Introduction

Free radicals are ubiquitous in most biological processes and, in unregulated concentrations, have been widely regarded as a cause of cell injury and death.[1−3] The need for detection of these radicals has become essential for the understanding of the mechanism of their generation for in vivo and in vitro systems. Hydroxyl ($^{\bullet}OH$), methyl ($^{\bullet}CH_3$), mercapto ($^{\bullet}SH$), hydroperoxy ($^{\bullet}O_2H$), superoxide ($O_2^{\bullet-}$), and nitric oxide (NO) are among the biologically relevant radicals that have been detected by spin trapping techniques (eq 1) using electron paramagnetic resonance (EPR) spectroscopy and synthetic nitrones.

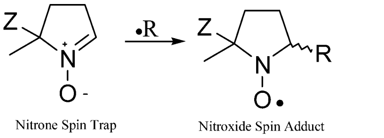

(1)

The role of these radicals in biological systems could be beneficial as well as detrimental. The C-centered radicals are regarded as both carcinogenic (e.g., generated from the reduction of halogenated hydrocarbons by NADPH-cytochrome P450)[2] and antitumor agents and are generated during oxidative metabolism of certain drugs such as 1,2-disubstituted hydrazines during microsomal oxidation in the presence of NADPH or by horseradish peroxidase-H_2O_2 catalyzed oxidation, as detected by EPR spin trapping using nitrone and nitroso spin traps.[4] Sulfur-centered or thiyl radicals are prevalent damaging agents from toxins such as the haemolytic drugs containing diphenyl disulfide[2] and are formed from the reaction of thiols (RSH) with several radicals, such as C-centered $^{\bullet}OH$, $^{\bullet}OR$, and $^{\bullet}O_2R$ radicals, for which a H-atom transfer reaction is exoergic.[2] Formation of $S^{\bullet-}$ has been detected by EPR spin trapping from the oxidation of sulfide ion by H_2O_2, and $S^{\bullet-}$ has been considered to be toxic to living systems.[5] The formation of $^{\bullet}O_2H$ results from the protonation of $O_2^{\bullet-}$ in aqueous systems, and $^{\bullet}O_2H$ is a better reducing agent than $O_2^{\bullet-}$ ($E^{\circ\prime} = -0.46$ and -0.33 V, respectively).[2] The hydroperoxyl radical is known to initiate lipid peroxidation processes and thereby forms $^{\bullet}OOR$ and H_2O_2 from organic peroxides (ROOH).[2] The superoxide radical anion, $O_2^{\bullet-}$, can be generated chemically from catechols as well as enzymatically from xanthine oxidase, β-nicotinamide adenine dinucleotide phosphate (NADPH) oxidase, or nitric oxide synthase (NOS), and $O_2^{\bullet-}$ is known to undergo dismutation to form H_2O_2, which is a source of more deleterious $^{\bullet}OH$ via Fenton chemistry.[2] Nitric oxide is produced from NOS[6,7] and plays an important physiological role in numerous biochemical processes such as neurotransmission, as a regulator of $O_2^{\bullet-}$ concentration via peroxy nitrite ONO_2^- formation, or as a vasodilator.[2]

Several papers have described the detection of $O_2^{\bullet-}$ and NO via the EPR spin trapping technique, using conventional nitrone spin traps[8] and Fe^{2+}-dithiocarbamates,[9] respectively. Recently,

* To whom correspondence should be addressed. F.A.V.: e-mail, villamena-1@medctr.osu-edu; fax, (614) 292-8454. C.M.H.: e-mail, hadad.1@osu.edu; fax, (614) 292-1685. J.L.Z.: e-mail, zweier-1@medctr.osu.edu; fax, (614)-247-7799.

† The Davis Heart and Lung Research Institute and College of Medicine, The Ohio State University.

‡ Department of Chemistry, The Ohio State University.

10.1021/jp0451492 CCC: $30.25
Published on Web 02/08/2005

alkoxycarbonyl nitrones such as ethoxycarbonyl-5-methyl-1-pyrroline *N*-oxide (EMPO)[10,11] and *tert*-butoxycarbonyl-5-methyl-1-pyrroline *N*-oxide (BocMPO)[12,13] and the alkoxyphosphoryl nitrones 5-diethyloxyphosphoryl-5-methyl-1-pyrroline *N*-oxide (DEPMPO)[14] and 5-diispropyloxyphosphoryl-5-methyl-1-pyrroline *N*-oxide (DIPPMPO) have been reported to trap $^{\bullet}OH$ and $O_2^{\bullet-}$. It is important to understand the chemical and physical basis that can influence the spin trapping efficiency of nitrones and the corresponding stability of their spin adducts, because these currently used spin traps are limited by their efficiency of trapping $O_2^{\bullet-}$ and by the stability of the $O_2^{\bullet-}$ adduct formed.

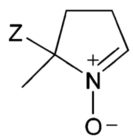

nitrone	Z
DMPO	-Me
EMPO	$-CO_2Et$
BocMPO	$-CO_2t$-Bu
DEPMPO	$-P(O)(OEt)_2$
DIPPMPO	-P(O)(O*i*-Pr)$_2$

We recently demonstrated[12,15,16] that a correlation of experimental kinetic data with theoretical results can provide insights into the effect of various substituents on the efficiency of spin trapping and spin adduct decay. There is a need to develop new spin traps with improved properties, as the alkoxyphosphorylated nitrones are by far the most efficient spin traps for $O_2^{\bullet-}$. However, they are limited by their ease of purification and limited shelf life, their sensitivity being a result of extensive and multiple hyperfine splitting from the ^{31}P.

This study aims to compare the relative reactivity of various radicals with a variety of cyclic nitrones in order to gain an understanding of the effect of substituents toward the spin trapping ability and the corresponding stabilities of their spin adducts. Using theoretical calculations, we also demonstrate, for the first time, a rationale as to why nitrones do not form stable spin adducts with NO. Furthermore, to date, computational modeling of the spin trapping event between reactive oxygen species and nitrones has led to barrierless processes.[16,17] Therefore, correlation of experimental kinetic parameters with calculated values from transition states have been lacking. By exploring a diverse set of radical trapping processes computationally, we hope to probe the existence of possible transition states for further analysis of reactivity trends. We report our studies with diverse radicals such as methyl, mercapto, hydroperoxy, superoxide anion, and NO herein.

II. Computational Methods

Density functional theory[18,19] was applied in this study to determine the optimized geometry, vibrational frequencies, and single-point energy of all stationary points.[20−23] The effect of solvation on the gas-phase single-point calculations was also investigated using the polarizable continuum model (PCM).[24−28] All of the electronic wave functions were found to be stable under the considered perturbations. All calculations were performed with Gaussian 98[29] at the Ohio Supercomputer Center or with Gaussian 98W (for Windows).[29] Single-point energies were obtained at the B3LYP/6-31+G(d,p) level using the optimized B3LYP/6-31G(d) geometries. Stationary points for both the nitrone spin traps and $^{\bullet}OH$ adducts have zero imaginary vibrational frequencies, as derived from a vibrational frequency analysis (B3LYP/6-31G(d)). A scaling factor of 0.9806 was used[30] for the zero-point vibrational energy (ZPE) corrections. For the minima, spin contamination for the adduct radicals was negligible: i.e., $0.75 < \langle S^2 \rangle < 0.76$. Spin densities (populations) were obtained from a natural population analysis (NPA) approach at the B3LYP/6-31G(d) level.[31] Only transition states of the NO adducts of various nitrones were located in this study, and attempts to locate the transition states of $O_2^{\bullet-}$, $^{\bullet}O_2H$, $^{\bullet}SH$, and $^{\bullet}CH_3$ adducts of DMPO were unsuccessful. All transition states for the NO adducts were confirmed to connect to reactants and products by incrementally displacing (typically 10%) the geometries along the reaction coordinate for the imaginary vibrational frequency in either direction, calculating the analytical force constants, and then optimizing to the corresponding minimum or by using an intrinsic reaction coordinate (IRC) search.[32,33] The $\langle S^2 \rangle$ values for the transition states showed minimal spin contamination of between 0.82 and 0.87. Free energies were obtained from the calculated thermal and entropic corrections at 298 K using the unscaled vibrational frequencies.

CHART 1: Acronyms of Spin Traps Used in the Study

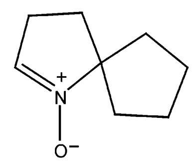

CPPO

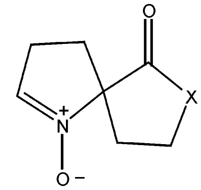

X	Acronym
O	CPCOMPO
N	TAMPO

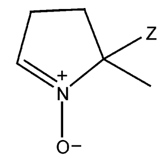

Z	Acronym
H	HMPO
CH_3	DMPO
CF_3	TFMPO
SO_2CH_3	MSMPO
$CONH_2$	AMPO
CO_2Et	EMPO
$PO(OEt)_2$	DEPMPO

III. Nomenclature

The general acronyms of spin traps used in this study are shown in Chart 1, while acronyms used for various configurational and conformational isomers of spin traps and their corresponding spin adducts are shown in Figures 1 and 2. The approximate optimized conformations of EMPO and DEPMPO are represented in Figure 1. Three conformations were obtained for both EMPO and DEPMPO.

Two configurations, i.e., cis and trans isomers, were assigned for all adducts, indicating the position of the substituents relative to the radical moiety (Figure 2). Each of the configurations for each spin adduct has three conformations corresponding to their respective nitrone. In some adducts, calculations were performed on *cis*-3 isomers in the presence and absence of intramolecular H-bonding. Table S1 of the Supporting Information summarizes the various orientations of the adduct substituents relative to the radical moieties expressed in terms of the dihedral angle

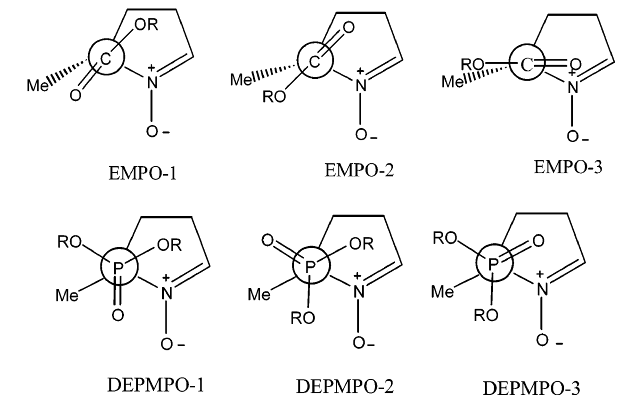

Figure 1. Approximate conformations of EMPO and DEPMPO spin traps and the respective naming system.

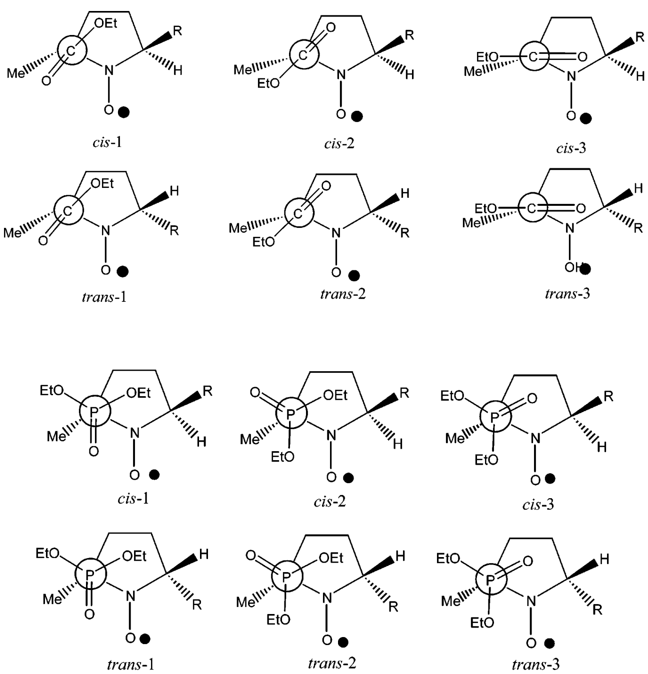

Figure 2. Approximate configurational and conformations isomers of various spin adducts with the corresponding naming system.

along the N−C−X−Y bond (where X−Y = O−O, S−H, N−O). Only one type of conformational isomer was predicted for both the cis and trans orientations of the MSMPO spin adducts, except for MSMPO-$O_2^{\bullet-}$ adducts, in which the optimized structure resulted in a nitrone-$O_2^{\bullet-}$ and methyl sulfoxyl radical according to eq 2. The naming system men-

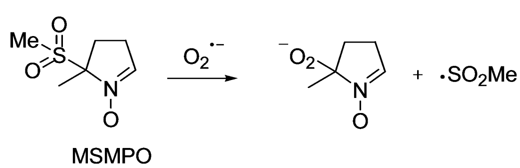

(2)

tioned above is applicable to all adducts except for the $O_2^{\bullet-}$ adduct which will be described in detail in the Superoxide Radical section of the Results and Discussion.

IV. Results and Discussion

Optimized Geometries. All bond lengths and angles for the relevant moieties for each nitrone and their respective adducts at the optimized geometry using the B3LYP/6-31G(d) level of theory have been extensively examined and, in general, showed no significant deviation from those reported experimentally using X-ray crystallography, as shown in Table 1. With the exception of the NO and SH adducts, the calculated average bond distances of 1.53 Å for C_{ring}−NO and 1.86 Å for C_{ring}−SH are much higher compared to their experimental bond distances of 1.35 Å[34] and 1.77 Å.[35] However, these experimental bond distance values were obtained from structures in which the NO and SH moieties are attached to an sp^2-hybridized carbon atom.

TABLE 1: Comparison of Selected X-ray Crystallographic Bond Lengths with Calculated Bond Lengths (B3LYP/6-31G(d))

bond	bond dist (Å) calcd range[a]	exptl
nitronyl C=N	1.30−1.31	1.291(2);[59] 1.307(2)[60]
nitronyl N−O	1.25−1.27	1.2987(16);[59] 1.294(1)[60]
nitroxyl C−N	1.47−1.49	1.50[61]
nitroxyl N−O	1.26−1.28	1.27[61]
P=O	1.47−1.49	1.4636(12);[59] 1.458(2)[62]
P−OR	1.59−1.64	1.580(1);[59] 1.575(2)[62]
P−C_{ring}	1.80−1.89	1.8276(16);[59] 1.813(3)[62]
C=O	1.20−1.25	1.196(10)[45]
C(O)−OR	1.33−1.37	1.337(15)[45]
C(O)−C_{ring}	1.53−1.56	1.496(18)[45]
C(O)−NH_2	1.35−1.37	1.331(3)[63]
MeS=O	1.46−1.47	1.448(3);[64]1.418(1)[65]
S−CH_3	1.81−1.82	1.752(3);[64]1.850(1)[65]
SO_2−C_{ring}	1.89−1.92	1.792(5);[64]1.833(2)[66]
C_{ring}−CF_3	1.53−1.55	1.530(3)[67]
	NO Adduct	
C_{ring}−N(=O)	1.51−1.55	1.345(7)[34 b]
N=O	1.19−1.22	1.279(6)[34]
	CH_3 Adduct	
C_{ring}−CH_3	1.52−1.53	1.465(10); 1.556(12)[60]
	O_2 Adduct	
C_{ring}−O_2	1.36−1.43	1.441(2)[47]
O−O	1.39−1.49	1.4599(17)[47]
	O_2H Adduct	
C_{ring}−O_2H	1.40−1.43	1.441(2)[47]
O−O	1.45−1.47	1.4599(17)[47]
O−H	0.97−0.98	1.02(3)[47]
	SH Adduct	
C_{ring}−SH	1.83−1.88	1.766(3)[35 b]
S−H	1.35−1.37	1.30(5)[35]

[a] For certain functional groups other than the nitronyl and nitroxyl groups, values are based on both nitrones and spin adducts. [b] On the sp^2 carbon atom.

General Trends. The order of increasing favorability for reaction, as judged by the average gas-phase free energies ΔG_{rxn} (in kcal/mol), for radical addition to nitrones is NO (14.57) < $O_2^{\bullet-}$ (−7.51) < $^{\bullet}O_2H$ (−13.92) < $^{\bullet}SH$ (−16.67) < $^{\bullet}CH_3$ (−32.17) < $^{\bullet}OH$ (−43.66) (see Table 2), which correlates in general (with the exception of $^{\bullet}SH$) with the reported reduction potentials ($E^{\circ\prime}$) for each radical (see Table 3 and Figure 3). The reported $E^{\circ\prime}$ values (in V) are NO (−0.80), $^{\bullet}SH$ (0.92), $O_2^{\bullet-}$ (0.94), $^{\bullet}O_2H$ (1.06), $^{\bullet}CH_3$ (1.90), and $^{\bullet}OH$ (2.31).[36] There is also a general correlation between the reported kinetic data and our calculated free energy of reactions. The reported apparent rate constants for the reaction of DMPO with these radicals are 10−50 M^{-1} s^{-1} with $O_2^{\bullet-}$,[12,37] 1.1 × 10^6 M^{-1} s^{-1} with $CH_3{}^{\bullet}CHOH$,[38] 2.6 × 10^8 M^{-1} s^{-1} with glutathiyl radical $GS^{\bullet}$,[39] and 1.93 × 10^9 M^{-1} s^{-1} with $^{\bullet}OH$.[15] The discrepancy between the order of kinetic reactivity of $GS^{\bullet}$ versus $CH_3{}^{\bullet}CHOH$ compared to our calculations may be due to the electronic and/

TABLE 2: Free Energies of Reaction[a] (ΔG_{rxn}, kcal/mol) for the Addition Reaction of Various Radicals to Nitrones at 298.15 K

nitrone	$^{\bullet}CH_3$	$^{\bullet}O_2H$	$^{\bullet}SH$	NO	$^{\bullet}OH$	$O_2^{\bullet -}$
HMPO	−31.14 (−31.88)	−12.23 (−6.20)	−16.17 (−13.04)	14.76 (14.05)	−42.58 (−37.55)	−3.72 (10.68)
DMPO	−30.24 (−31.47)	−12.82 (−7.91)	−15.47 (−12.80)	15.06 (13.98)	−42.07 (−38.05)	−3.38 (12.57)
CPPO	−30.15 (−31.20)	−12.93 (−4.85)	−15.00 (−12.32)	14.82 (13.74)	−42.27 (−38.31)	−2.85 (14.75)
TAMPO	−31.48 (−32.05)	−13.69 (−6.37)	−16.28 (−13.22)	15.56 (15.24)	−42.92 (−38.18)	−9.13 (9.69)
TFMPO	−33.24 (−34.00)	−14.65 (−6.15)	−17.10 (−13.87)	15.26 (14.64)	−43.40 (−39.02)	−11.35 (8.67)
CPCOMPO	−32.10 (−32.99)	−13.45 (−5.19)	−16.37 (−13.43)	15.64 (15.20)	−43.01 (−38.59)	−11.12 (9.20)
MSMPO	−35.57 (−35.70)	−17.1 (−7.30)	−19.18 (−15.17)	12.92 (13.38)	−46.78 (−41.32)	n/a
AMPO	−30.81 (−32.31)	−12.02 (−6.94)	−14.88 (−12.87)	16.24 (15.08)	−41.41 (−38.59)	−16.75[b] (3.76)
EMPO	−32.69 (−34.14)	−14.57 (−10.07)	−17.25 (−14.91)	13.51 (12.38)	−44.04 (−40.30)	−7.70 (8.88)
DEPMPO	−34.26 (−33.10)	−15.7 (−8.53)	−17.77 (−14.10)	11.96 (13.50)	−45.53 (−39.19)	−10.82 (11.31)
av	**−32.17 (−32.88)**	**−13.92 (−6.95)**	**−16.55 (−13.57)**	**14.57 (14.12)**	**−43.66 (−38.91)**	**−7.51 (9.95)**
std dev	1.78 (1.40)	1.60 (1.57)	1.33 (0.93)	1.35 (0.93)	1.76 (1.13)	3.67 (3.04)

[a] The most exoergic reaction was considered for reactions that produce diastereomeric adducts. Values in parentheses are ΔG_{rxn} values based on single-point energy calculations with the polarizable continuum model (PCM) at the B3LYP/6-31+G(d,p) level using water as a solvent. Adducts with intramolecular H-transfer reaction and nucleophilic addition to carbonyl carbon, such as in the case of AMPO−O_2 *cis*-3B and EMPO−O_2 *cis*-3B, respectively, were not considered. [b] Outlier; not included in the average value.

TABLE 3: Average Free Energy of Reaction ΔG_{rxn} for Radical Adduct Formation with Nitrones at 298.15 K and Their Corresponding Reduction Potential $E°'$

radical	av ΔG_{rxn} (kcal/mol)	half-reaction	$E°'$, V	ref
$^{\bullet}OH$	−43.66	$^{\bullet}OH$, H^+/H_2O	2.31	36
$^{\bullet}CH_3$	−32.17	$H_3CH_2C^{\bullet}$, H^+/CH_3CH_3	1.90	36
$^{\bullet}SH$	−16.55	$^{\bullet}S^-$, H^+/SH^-	0.92	68
$^{\bullet}O_2H$	−13.92	$^{\bullet}OOH$, H^+/H_2O_2	1.06	36
$O_2^{\bullet -}$	−7.51	$O_2^{\bullet -}$, $2H^+/H_2O_2$	0.94	36
NO	14.57	$NO/^3NO^-$	−0.80	69

or steric effect of the glutathione and hydroxyl groups on the atom bearing the unpaired electron. Recently, the rate constant for the trapping reaction of BocMPO with $O_2^{\bullet -}$ at pH 7.0 was reported to be 75.0 ± 10.5 M^{-1} s^{-1}, while at pH 5.0, in which $^{\bullet}O_2H$ is predominant, the rate constant is 239.2 ± 10.5 M^{-1} s^{-1}.[40] Nitric oxide has been reported to only give artifactual spin adducts,[41,42] indicating that NO is unreactive toward nitrones under normal conditions. These experimental rate constants (except for GS$^{\bullet}$) also correlate with their correspondence to theoretically calculated free energies of reactions.

Boyd and Boyd reported[43] the order of increasing formation energies at the MP2/6-31G(d,p)//HF/6-31G(d) level of theory: for the nitroso HN═O spin adducts (ΔE_{MP2} in kcal/mol) NO (7.8) < $^{\bullet}O_2H$ (−8.4) < $^{\bullet}SH$ (−21.5) < $^{\bullet}OH$ (−32.6) < $^{\bullet}CH_3$ (−53.1); for $CH_3N{=}O$ (ΔE_{MP2} in kcal/mol) NO (8.0) < $^{\bullet}O_2H$ (−7.5) < $^{\bullet}SH$ (−18.2) < $^{\bullet}OH$ (−35.8) < $^{\bullet}CH_3$ (−50.1). The endothermicity of the NO reaction with nitroso compounds is consistent with our prediction for the NO reaction with DMPO-type nitrones. However, the order for exothermicity for $^{\bullet}OH$ (−32.6 kcal/mol) and $^{\bullet}CH_3$ (−53.9 kcal/mol) reaction with HN═O is reversed compared to that found in this study using the DMPO-type nitrone. It has also been reported[17] that the addition of $^{\bullet}OH$ to the nitrone $H_2C{=}NHO$ is the most exothermic, ΔE_{MP2} = −244 kJ/mol (−58.3 kcal/mol), followed by the $^{\bullet}CH_3$ reaction with ΔE_{MP2} = −221 kJ/mol (−52.8 kcal/mol) and $^{\bullet}O_2H$ reaction with ΔE_{MP2} = −141 kJ/mol (−33.7 kcal/mol) at the MP2/6-31G(d,p)//HF/6-31G(d) level. This trend of radical reactivity is consistent with our prediction at the B3LYP/6-31+G(d,p)//B3LYP/6-31G(d) level.

Methyl Radical. The reaction free energies for the $^{\bullet}CH_3$ addition to nitrones indicate that the formations of cis $^{\bullet}CH_3$ adducts are more exoergic compared to the formation of their respective trans $^{\bullet}CH_3$ adducts by less than 1 kcal/mol, except for the formation of TAMPO-CH_3 cis, which is more favored compared to its trans analogue by about 6 kcal/mol (see Table 4). In comparison to the addition of $^{\bullet}CH_3$ to nitrones, the addition of $^{\bullet}OH$ to various nitrones mostly favors the formation of trans $^{\bullet}OH$ adducts also by less than 1 kcal/mol (except for the

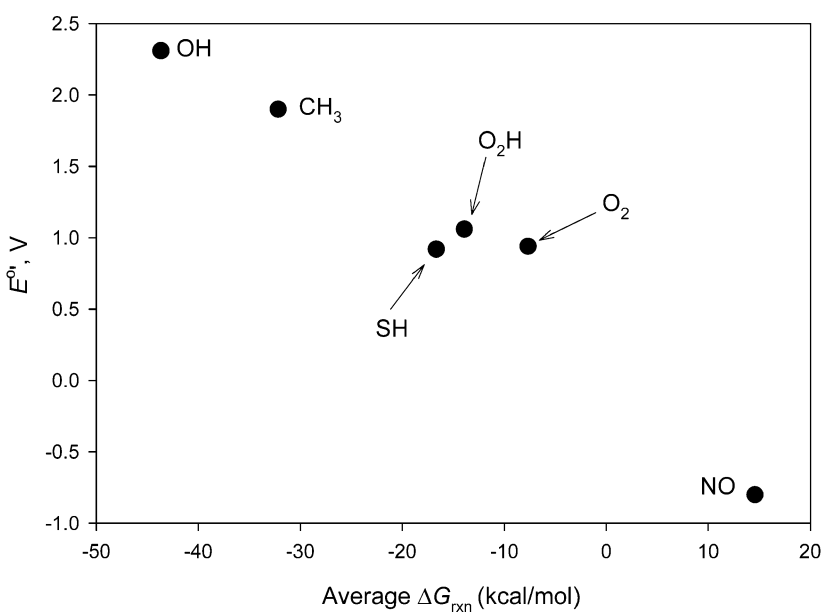

Figure 3. Plot of experimental standard reduction potentials ($E°'$) versus the average free energies (ΔG_{rxn}) for adduct formation with the nitrones studied here.

TABLE 4: Relative Energy[a] ($E_{0,tot}$) and Enthalpy[b] (H_{298K}) of the Theoretically Optimized Spin Adduct Structures at the B3LYP/6-31+G(d,p)//B3LYP/6-31G(d) Level in the Gas Phase and PCM Model for Water[c]

	spin adduct							
	$^{\bullet}CH_3$		$^{\bullet}O_2H$		$^{\bullet}SH$		NO	
entry	rel *E*	rel *H*	rel *E*	rel *H*	rel *E*	rel *H*	rel *E*	rel *H*
TAMPO cis	0.0 (0.0)	0.0 (0.0)	0.0 (0.0)	0.0 (0.0)	0.0 (0.0)	0.0 (0.0)	0.0 (0.0)	0.0 (0.0)
TAMPO trans	6.2 (5.4)	6.2 (5.4)	1.3 (2.8)	1.1 (2.7)	−1.5 (−1.6)	−1.5 (−1.6)	−2.6 (−1.3)	−2.5 (−1.3)
TFMPO cis	0.0 (0.0)	0.0 (0.0)	0.0 (0.0)	0.0 (0.0)	0.0 (0.0)	0.0 (0.0)	0.0 (0.0)	0.0 (0.0)
TFMPO trans	0.8 (0.9)	0.9 (0.9)	−3.2 (0.2)	−3.0 (0.3)	−2.5 (−1.3)	−2.4 (−1.2)	−2.0 (−1.1)	−2.0 (−1.0)
CPCOMPO cis	0.0 (0.0)	0.0 (0.0)	0.0 (0.0)	0.0 (0.0)	0.0 (0.0)	0.0 (0.0)	0.0 (0.0)	0.0 (0.0)
CPCOMPO trans	0.5 (0.7)	0.6 (0.8)	0.5 (1.5)	0.3 (1.4)	−1.8 (−1.7)	−1.8 (−1.7)	−2.6 (−1.1)	−2.5 (−1.1)
MSMPO cis	0.0 (0.0)	0.0 (0.0)	0.0 (0.0)	0.0 (0.0)	0.0 (0.0)	0.0 (0.0)	0.0 (0.0)	0.0 (0.0)
MSMPO trans	0.8 (0.9)	0.8 (0.9)	−2.6 (−0.9)	−2.5 (−0.1)	−1.2 (−1.0)	−1.2 (−1.0)	−1.5 (0.1)	−1.5 (0.0)
AMPO*cis*-2a	0.0 (0.0)	0.0 (0.0)	0.0 (0.0)	0.0 (0.0)	0.0 (0.0)	0.0 (0.0)	0.0 (0.0)	0.0 (0.0)
AMPO*cis*-2b	n/a	n/a	4.0 (−1.7)	3.8 (−1.9)	1.6 (0.1)	1.5 (0.0)	0.1 (0.1)	0.2 (0.2)
AMPO*cis*-3	n/a	n/a	6.6 (0.8)	6.4 (0.6)	n/a	n/a	n/a	n/a
AMPO*trans*-2[d]	0.5 (0.5)	0.6 (0.6)	0.8 (0.7)	0.6 (0.6)	−0.8 (−0.4)	−0.8 (−0.4)	−1.6 (−1.0)	−1.6 (−1.0)
EMPO *cis*-1	0.0 (0.0)	0.0 (0.0)	0.0 (0.0)	0.0 (0.0)	0.0 (0.0)	0.0 (0.0)	0.0 (0.0)	0.0 (0.0)
EMPO *cis*-2	0.1 (0.8)	0.1 (0.8)	4.7 (0.6)	4.4 (0.2)	−1.7 (−0.9)	−1.6 (−0.8)	−2.0 (0.4)	−2.0 (0.4)
EMPO *cis*-3	0.3 (0.0)	0.3 (0.0)	1.0 (−0.8)	0.9 (−0.9)	−0.6 (−0.9)	0.5 (−0.9)	n/a	n/a
EMPO *trans*-1	0.4 (0.5)	0.5 (0.5)	2.5 (−1.7)	2.2 (−2.0)	−2.7 (−2.4)	−2.6 (−2.2)	−3.1 (−1.6)	−3.1 (−1.6)
EMPO *trans*-2	0.8 (1.3)	0.8 (1.3)	3.3 (−1.8)	3.1 (−2.1)	0.1 (−0.7)	0.1 (−0.7)	−2.6 (−0.6)	−2.6 (−0.6)
EMPO *trans*-3a	0.8 (1.0)	0.9 (1.1)	1.3 (−2.7)	1.2 (−2.8)	n/a	n/a	n/a	n/a
EMPO *trans*-3b	n/a	n/a	0.1 (−0.1)	0.1 (−0.2)	n/a	n/a	n/a	n/a
EMPO *trans*-3c	n/a	n/a	2.9 (−1.7)	2.5 (−2.0)	n/a	n/a	n/a	n/a
DEPMPO *cis*-1	0.0 (0.0)	0.0 (0.0)	0.0 (0.0)	0.0 (0.0)	0.0 (0.0)	0.0 (0.0)	0.0 (0.0)	0.0 (0.0)
DEPMPO *cis*-2	−0.9 (0.5)	−0.8 (0.6)	0.1 (0.6)	0.1 (0.6)	0.8 (2.3)	0.9 (2.4)	0.1 (0.0)	0.2 (0.0)
DEPMPO *cis*-3a	−2.6 (−0.6)	−2.4 (−0.4)	3.9 (0.0)	3.6 (−0.3)	−1.0 (0.1)	−0.9 (0.2)	−0.2 (0.2)	−0.3 (0.1)
DEPMPO *cis*-3b	n/a	n/a	2.6 (2.1)	2.3 (1.9)	−2.3 (0.5)	−2.1 (0.6)	n/a	n/a
DEPMPO *trans*-1	0.5 (0.6)	0.7 (0.7)	0.6 (0.8)	0.6 (0.8)	−0.6 (−0.4)	−0.5 (−0.3)	−0.8 (−1.4)	−0.8 (−1.4)
DEPMPO *trans*-2	−0.1 (0.4)	0.1 (0.5)	−0.3 (0.1)	−0.3 (0.1)	−1.5 (−0.5)	−1.3 (−0.3)	−1.7 (−1.7)	−1.7 (−1.8)
DEPMPO *trans*-3	−1.8 (0.1)	−1.7 (0.3)	2.2 (−1.5)	1.8 (−1.8)	−0.3 (−0.1)	−0.3 (0.0)	−3.1 (−1.9)	−3.2 (−1.9)

[a] Relative to reactants, in kcal/mol. $E_{0,rxn}$ are bottom-of-the-well energies and are ZPE uncorrected. [b] Relative values are in kcal/mol relative to their respective isomer cis or *cis*-1. [c] Values in parentheses are relative energies based on single-point energy calculations with the polarizable continuum model (PCM) at the B3LYP/6-31+G(d,p) level using water as a solvent. [d] All initial structures of AMPO *trans*-1 *and trans*-3 adducts optimized to AMPO *trans*-2, except for the AMPO−$O_2^{\bullet -}$ adduct.

alkoxyphosphorylated nitrones, which favor the cis isomers by about 4 kcal/mol).[15,16]

The most negative free energy of reaction was observed for the methyl sulfonylated nitrone MSMPO, with an average ΔG_{rxn} of −35.4 kcal/mol, and with only a 0.4 kcal/mol difference between the cis and trans adducts. The order of decreasing ΔG_{rxn} (kcal/mol) for the $^{\bullet}CH_3$ addition to various nitrones is MSMPO-CH_3 cis (−35.6) > DEPMPO-CH_3 *cis*-3 (−34.3) > TFMPO-CH_3 cis (−33.2) > EMPO-CH_3 *cis*-1 (−32.7) > CPCOMPO-CH_3 cis (−32.1) > TAMPO-CH_3 cis (−31.5) > HMPO-CH_3 (−31.1) > AMPO-CH_3 *cis*-2 (−30.8) > DMPO-CH_3 (−30.2) = CPPO-CH_3 (−30.2) (Table S2 in the Supporting Information). The difference in the dipole moments between the most favored cis and trans adducts is insignificant. These small differences in formation energies and dipole moments for both cis and trans adducts of $^{\bullet}CH_3$ may indicate that both isomers are favored at equilibrium. Several C-centered radicals have been trapped by various alkoxycarboxylated and alkoxyphosphorylated nitrones; e.g., the $CH_3{}^{\bullet}CHOH$ radical generated from a Fenton−ethanol mixture gave EPR spectra characteristic for the presence of a mixture of cis and trans isomers, as confirmed by spectral simulation techniques.[15] Natural population analysis (NPA)[31] of $^{\bullet}CH_3$ shows that the excess spin density (population) is localized 100% on the C atom, while after adduct formation with various nitrones, the electron is delocalized mostly on the N−O moiety, with the N and O atoms having about an average of 45% and 51% of the spin densities, respectively (Table S8 in the Supporting Information).

Single-point energy calculations with the PCM method at the B3LYP/6-31+G(d,p) level using water as a solvent shows the same qualitative trend in ΔG_{rxn} as in the gas phase, i.e., MSMPO being the most exoergic with −35.7 kcal/mol, while DMPO and CPPO are the least exoergic with ΔG_{rxn} values of −31.47 and −31.20 kcal/mol, respectively. The average ΔG_{rxn} of addition of $^{\bullet}CH_3$ with various nitrones in aqueous solution (−32.88 ± 1.40 kcal/mol) was predicted to be similar to that observed in the gas phase (−32.17 ± 1.78 kcal/mol), and the formation of the cis adduct is also preferred in water, similar to that predicted in the gas phase (Table 2).

Mercapto Radical. Similar to the formation of $^{\bullet}OH$ adducts,[16] the formation of trans $^{\bullet}SH$ adducts is more preferred in most cases than the cis adducts by 1−3 kcal/mol (Table 4). The order of decreasing ΔG_{rxn} (kcal/mol) for the $^{\bullet}SH$ addition to various nitrones is MSMPO-SH trans (−19.2) > DEPMPO-SH *cis*-3b (−17.8) > EMPO-SH *trans*-1 (−17.3) > TFMPO-SH trans (−17.1) > CPCOMPO-SH trans (−16.4) > TAMPO-SH trans (−16.3) > HMPO-SH (−16.2) > DMPO-SH (−15.47) > CPPO-SH (−15.0) > AMPO-SH trans (−14.9) (see Table S3 of the Supporting Information). The formation of DEPMPO-SH *cis*-3b is the most preferred product for $^{\bullet}SH$ addition to DEPMPO by ∼2.0 kcal/mol, which also exhibits a relatively weak intramolecular H-bonding interaction between the P═O and S−H moieties, although the P═O- - -H−S bond distance is relatively long, i.e., 2.30 Å, compared to P═O- - -H−O bond distances[16] of 1.92 Å for DEPMPO-OH *cis*-3. This difference in H-bond distances for the $^{\bullet}SH$ and $^{\bullet}OH$ adducts could be due to the difference in the relative acidities and polarizability of RSH compared to those of ROH; for example, the pK_a values for EtOH and EtSH are 15.9 and 10.61,[44] respectively, and the polarizability of EtSH (7.41×10^{-24} cm^3) is higher compared to that of EtOH (5.41×10^{-24} cm^3).[45] Moreover, the C═O- - -H−S bond distance is 2.47 Å for EMPO-SH *cis*-3, which is

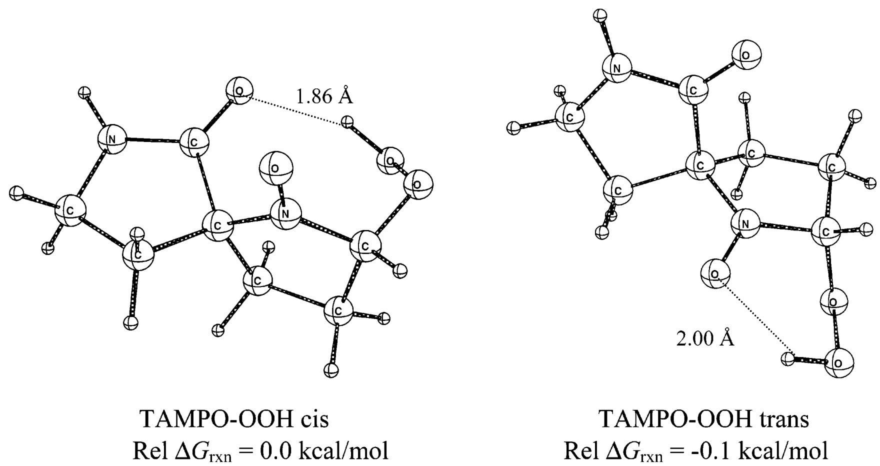

Figure 4. Views of the B3LYP/6-31G(d) optimized geometry of TAMPO-OOH cis (left) and TAMPO-OOH trans (right), showing the presence of intramolecular H-bonding interactions.

longer than the C═O- - -H−O bond distances[16] of 2.07 Å predicted for EMPO-OH *cis*-3. The H-bonding ability of an S−H donor has been previously observed[46] and was found to exhibit S−H- - -X interactions with various acceptors involving X = O, S, N, Cl, with a mean intermolecular H- - -O distance of 2.34(4) Å, which was gathered from various X-ray crystallographic data. This experimental average of 2.34(4) Å is close to that calculated for EMPO-SH *cis*-3 of 2.47 Å. The average spin densities on N and O of the nitroxyl group are 42% and 51%, respectively, while spin density is localized on the S atom of •SH (100%) before trapping. Dipole moments of the cis isomers are significantly much higher compared to that of the thermodynamically preferred trans adduct isomers (similar to that predicted for the •OH adducts), with the exception of those adducts that exhibit intramolecular H-bonding that are thermodynamically favored.

Calculations with the aqueous PCM model gave an average ΔG_{rxn} for the addition of •SH to nitrones of -13.57 ± 0.93 kcal/mol, which is less exoergic compared to the average ΔG_{rxn} in the gas phase of -16.55 ± 1.33 kcal/mol. The formation of trans isomers from all nitrones is preferred, similar to that predicted in the gas phase, with the exception of DEPMPO-SH *cis*-3b (with H-bonding), which is less exoergic compared to the formation of DEPMPO-SH *trans*-1 in water. Furthermore, the order of reactivity of various nitrones to •SH follows the same qualitative trend observed in the gas phase, with MSMPO being the most reactive while AMPO, CPPO, and DMPO are the least reactive (Table 2).

Hydroperoxy Radical. The spin density distribution on •OOH shows 73% on the terminal O and 27% on the internal O. However, the spin densities are almost evenly distributed within the N−O moiety after spin trapping by nitrones with 43% and 52% spin densities on the N and O atoms, respectively. The O−O bond distance in the •O_2H is shorter, i.e., 1.33 Å, compared to the O−O bond distance in the •O_2H adducts, which has a mean average of 1.455(2) Å, similar to that observed in **2** of 1.4599(17) Å.[47]

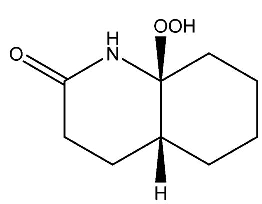

2

Several adducts with intramolecular H-bonding (−OOH- - -X) are predicted that include −OOH- - -O−N, −OOH- - -O═C, and −OOH- - -O═S H-bonding modes. Of all of the •O_2H adducts studied, the lactam TAMPO-OOH cis isomer (which is also the more thermodynamically favored isomer over its trans isomer by 1.1 kcal/mol) was predicted to exhibit the shortest H-bond with a −OOH- - -O═C bond distance of 1.86 Å, compared to its trans isomer with a −OOH- - -O−N bond distance of 2.00 Å (Figure 4). The −OOH- - -O−N bonding mode was predicted in both cis and trans isomers for most of the isomers, with a mean average distance of 2.00 Å. Interestingly, the −OOH- - -O−N bonding mode which has a longer H- - -O bond distance of 2.00 Å in AMPO-OOH *cis*-2a is more thermodynamically preferred by about 6.2 kcal/mol than the AMPO-OOH *cis*-3 isomer with an H- - -O distance of 1.90 Å due to the −OOH- - -O═C bonding. Similarly, this behavior was also observed in EMPO-OOH *cis*-3 (−OOH- - -O═C) versus EMPO-OOH *cis*-1 (−OOH- - -O−N). The −OOH- - -O═P bonding in the case of DEPMPO-OOH *cis*-3b is less preferred compared to some of its adducts that exhibit −OOH- - -O−N bonding (e.g., DEPMPO-OOH *trans*-2), considering that, in the •OH adducts, the −OH- - -O═C and −OH- - -O═P bonding motifs are usually the most preferred configuration. Table S4 shows the thermodynamic parameters for the formation of •OOH adducts. The order of decreasing ΔG_{rxn} (kcal/mol) is as follows: MSMPO-OOH trans (−17.1) > DEPMPO-OOH trans (−15.7) > TFMPO-OOH trans (−14.7) > EMPO-OOH *trans*-3b (−14.6) > TAMPO-OOH trans (−13.7) > CP-COMPO-OOH trans (−13.5) > CPPO-OOH (−12.9) > DMPO-OOH (−12.8) > HMPO-OOH (−12.2) > AMPO-OOH *trans*-2 (−12.0). Table 5 shows the O- - -H bond distances of various cis and trans •OOH adducts. Analyses of the dipole moments of the adducts indicate that, in general, the trans isomer, which is the more preferred configuration, has a lower dipole moment than the cis isomer.

The favorability for formation of cis •OOH adducts over trans varies in the aqueous phase compared to the gas phase for various nitrones (Table 4). For example, the TAMPO-OOH cis isomer is more favored, while the formation of trans •OOH adducts of EMPO, DEPMPO, and MSMPO are more preferred, in general. The preference for intramolecular H-bonding in the aqueous phase has changed for AMPO-OOH *cis*-2a, EMPO-OOH *cis*-1 and *cis*-2, and DEPMPO-OOH *cis*-3b, as the corresponding adducts without intramolecular H-bonding were more favored. The predicted order of reactivity of •OOH to nitrones was also perturbed in solution; i.e., the order of

TABLE 5: Hydrogen Bond Distances (Å) in the B3LYP/6-31G(d) Optimized Geometries of Various Hydroperoxyl Adducts

OOH adduct	H-bond dist (Å)	type
HMPO	2.54	−OOH- - -O−N
DMPO	1.99	−OOH- - -O−N
CPPO	2.00	−OOH- - -O−N
TAMPO cis	1.86	−OOH- - -O=C
TAMPO trans[a]	2.00	−OOH- - -O−N
TFMPO cis	2.39	−OOH- - -O−N
TFMPO trans[b]	2.00	−OOH- - -O−N
CPCOMPO cis	1.93	−OOH- - -O=C
CPCOMPO trans[b]	2.02	−OOH- - -O−N
MSMPO cis	1.95	−OOH- - -O=S
MSMPO trans[b]	2.01	−OOH- - -O−N
AMPO *cis*-2a	2.00	−OOH- - -O−N
AMPO *cis*-3	1.90	−OOH- - -O=C
AMPO *trans*-2[b]	2.00	−OOH- - -O−N
EMPO *cis*-1	1.98	−OOH- - -O−N
EMPO *cis*-3	2.00	−OOH- - -O=C
EMPO *trans*-3b[b]	1.99	−OOH- - -O−N
DEPMPO *cis*-1	1.97	−OOH- - -O−N
DEPMPO *cis*-2	2.00	−OOH- - -O−N
DEPMPO *cis*-3b	1.91	−OOH- - -O=P
DEPMPO *trans*-1	2.02	−OOH- - -O−N
DEPMPO *trans*-2[b]	2.00	−OOH- - -O−N

[a] ΔG_{rxn} is only 0.1 kcal/mol more exoergic relative to the cis isomer. [b] Most preferred configuration relative to its respective isomers based on ΔG_{rxn}.

decreasing ΔG_{rxn} (kcal/mol) has changed to EMPO-OOH *trans*-3a (−10.07) > DEPMPO-OOH *trans*-3 (−8.53) > DMPO-OOH (−7.91) > MSMPO-OOH trans (−7.3) > AMPO-OOH *cis*-2b (−6.94) > TAMPO-OOH cis (−6.37) > HMPO-OOH (−6.20) > TFMPO-OOH cis (−6.15) > CPCOMPO-OOH trans (−5.19) > CPPO-OOH (−4.85). There is a significant difference in the average ΔG_{rxn} (−6.95 ± 1.57 kcal/mol) for the addition of •OOH to nitrones in water, which is significantly less exoergic compared to the average ΔG_{rxn} in the gas phase of −13.92 ± 1.60 kcal/mol (Table 2).

Superoxide Radical. By symmetry, there is an equal distribution of spin densities between the two O atoms of $O_2^{\bullet-}$. Figure 5 shows the two possible projections, **A** and **B**, of the O−O moiety with respect to N−O in the $O_2^{\bullet-}$ adducts, while Table 6 shows the relative energies and dihedral angles of the −O−O group relative to the −N−O group. The thermodynamically preferred $O_2^{\bullet-}$ adducts of HMPO, DMPO, and CPPO have projections similar to **B** and yielded significantly higher spin density distributions on the nitronyl N and slightly higher spin density on the nitronyl O but a lower spin distribution on the O−O moiety compared to projection **A** (see Table 7). As also shown in our previous studies involving substituted nitrones,[48] there is a significant difference in spin density distribution among the conformational isomers. Figure 6 shows the dependence of N atom spin density distribution on the orientation of the superoxide group relative to the N−O projection in the DMPO-O_2 adduct (see Figure 6 for the pictorial orientation of these dihedral angles). Three local minima were predicted for DMPO-O_2 according to Figure 6, in which the spin density distribution on N is maximum at a O−O−C−N dihedral angle of 315° close to the $\Delta E_{o,rxn}$ value where the formation of DMPO-O_2 is most exoergic, corresponding to a O−O−C−N dihedral angle of 283.6°. The lowest spin density on N was predicted at a dihedral angle of 67.5°, close to the dihedral angle of 22.5°, in which the $\Delta E_{o,rxn}$ value is least negative. The cis-vicinal orientation of N−O relative to the −O−O group is least favored, while the trans-vicinal conformation is more energetically preferred. This high distribution of spin density on the N in the trans-vicinal conformation could be due to the effective overlap of the antibonding π^* SOMOs of the nitroxyl and the superoxide groups, which parallels that of the Karplus-type relationship observed in trans-vicinal H's, which exhibit higher coupling constants compared to the cis-vicinal configurations.[49]

It is assumed that the $O_2^{\bullet-}$adduct is formed initially, since the pK_a of $HO_2^{\bullet}$ is approximately 4.8, and $O_2^{\bullet-}$ is predominant at neutral pH.[50] The relatively high spin density distribution and negative charge (as indicated by the NPA charge distribution) on the terminal O of the R−O−O− group may exhibit reactivity similar to that of the $O_2^{\bullet-}$ ion. In the gas phase as well as in the aqueous solution,[51−53] it has been demonstrated that $O_2^{\bullet-}$

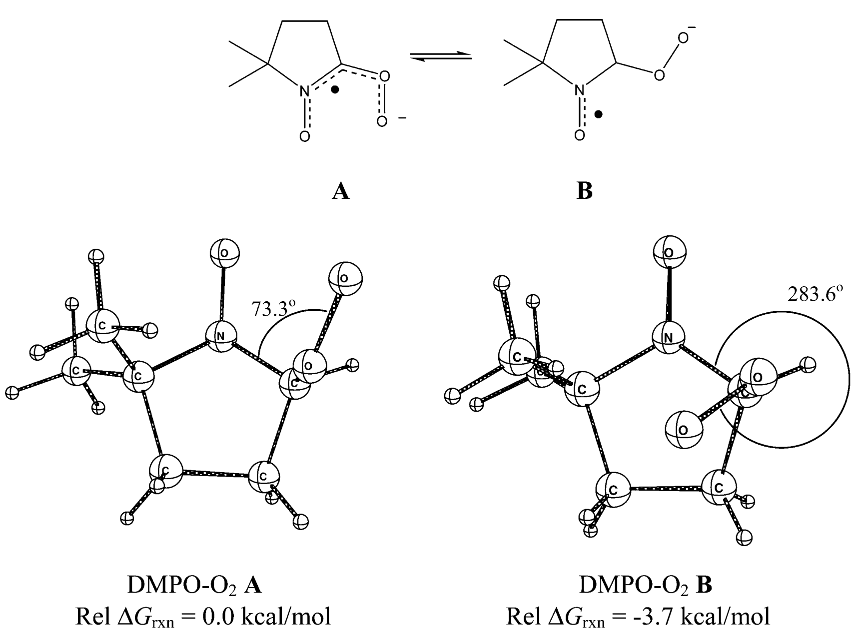

Figure 5. Views of the B3LYP/6-31G(d) optimized geometry of DMPO-O_2 (**A**, left) and DMPO-O_2 (**B,** right), showing the orientation of the superoxide moiety with respect to the N−O group.

TABLE 6: Relative Energy[a] ($E_{0,tot}$) and Enthalpy[b] (H_{298K}) of the Theoretically Optimized Superoxide Adduct Structures at the B3LYP/6-31+G(d,p)//B3LYP/6-31G(d) Level and Their Corresponding Dihedral Angles

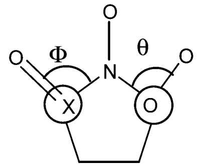

$O_2^{\bullet-}$ adduct[a]	Φ	θ	rel *E*	rel *H*
HMPO A	n/a	73.1	0.0 (0.0)	0.0 (0.0)
HMPO B	n/a	284.5	−4.3 (1.0)	−4.2 (1.2)
DMPO A	n/a	73.3	0.0 (0.0)	0.0 (0.0)
DMPO B	n/a	283.6	−4.7 (−0.1)	−4.5 (0.2)
CPPO A	n/a	64.2	0.0 (0.0)	0.0 (0.0)
CPPO B	n/a	288.4	−3.6 (−0.5)	−3.4 (−0.4)
TAMPO *cis*-B	307.8	187.7	0.0 (0.0)	0.0 (0.0)
TAMPO *trans*-A	285.4	60.8	−4.6 (2.5)	−4.0 (3.2)
TAMPO *trans*-B	282.7	285.4	−8.0 (0.4)	−7.5 (0.9)
TFMPO *cis*-A	n/a	77.0	0.0 (0.0)	0.0 (0.0)
TFMPO *cis*-B	n/a	295.8	−1.8 (−1.4)	−1.9 (−1.5)
TFMPO *trans*-A	n/a	67.8	−5.8 (−1.7)	−5.7 (−1.5)
TFMPO *trans*-B	n/a	194.0	−8.0 (−2.2)	−7.9 (−1.8)
CPCOMPO *cis*-B	312.3	188.3	0.0 (0.0)	0.0 (0.0)
CPCOMPO *trans*-A	281.2	60.1	−4.9 (1.4)	−4.3 (2.0)
CPCOMPO *trans*-B	279.8	196.0	−4.6 (1.5)	−4.2 (1.9)
AMPO *cis*-1A	167.0	48.9	0.0 (0.0)	0.0 (0.0)
AMPO *cis*-1B	215.8	190.4	14.6 (11.6)	14.5 (11.6)
AMPO *cis*-1C	166.8	57.4	3.4 (−2.0)	3.6 (−1.8)
AMPO *cis*-2B	134.5	196.7	9.0 (4.1)	9.1 (4.2)
AMPO *cis*-3B	171.3	283.8	−1.5 (−0.7)	−1.5 (−0.7)
AMPO *trans*-A	227.0	75.2	13.6 (8.7)	13.9 (9.0)
AMPO *trans*-B	222.5	281.2	12.1 (6.8)	12.5 (7.2)
MAMPO *cis*-H	287.0	158.9	0.0 (0.0)	0.0 (0.0)
MAMPO *cis*	258.7	77.0	21.3 (13.2)	22.6 (14.4)
EMPO *cis*-1A	83.2	64.5	0.0 (0.0)	0.0 (0.0)
EMPO *cis*-2A	232.5	73.0	−3.2 (−3.0)	−3.0 (−2.9)
EMPO *cis*-1B	74.7	196.0	−4.1 (−1.6)	−4.1 (−1.5)
EMPO *cis*-2B	228.4	202.5	−2.2 (−0.3)	−2.2 (−0.3)
EMPO *cis*-3B	64.2	291.0	−9.2 (−4.3)	−9.1 (−4.2)
EMPO *trans*-1A	129.7	71.7	−1.6 (−4.0)	−1.6 (−4.0)
EMPO *trans*-1B	262.4	193.2	−5.3 (−6.6)	−5.3 (−6.6)
EMPO *trans*-2B	269.5	284.5	−6.0 (−5.1)	−5.7 (−4.8)
DEPMPO *cis*-1A	84.9	78.6	0.0 (0.0)	0.0 (0.0)
DEPMPO *cis*-2A	126.1	76.8	3.3 (4.8)	3.4 (4.9)
DEPMPO *cis*-3A	274.3	72.7	2.1 (1.9)	2.1 (1.9)
DEPMPO *trans*-1A	90.5	74.3	4.1 (1.1)	4.2 (1.1)
DEPMPO *trans*-2A	157.7	71.4	3.1 (1.6)	3.2 (1.7)
DEPMPO *trans*-3A	293.7	72.1	1.5 (1.4)	1.5 (1.4)
DEPMPO *cis*-1B	81.4	284.0	−2.2 (−0.1)	−2.0 (0.0)
DEPMPO *cis*-2B	260.1	190.6	4.9 (3.1)	4.9 (3.1)
DEPMPO *trans*-1B	89.1	195.4	2.0 (0.2)	1.9 (0.1)
DEPMPO *trans*-2B	155.1	193.1	1.6 (0.5)	1.6 (0.5)
DEPMPO *trans*-3B	299.3	194.0	0.5 (0.8)	0.5 (0.7)

[a] Adducts with conformation A have $\theta = 48.9-78.6°$, while those with conformation B have $\theta = 187.7-295.8°$.

can undergo reversible nucleophilic addition to the carbonyl carbon (eq 3). Theoretical analysis of EMPO-O_2 adducts

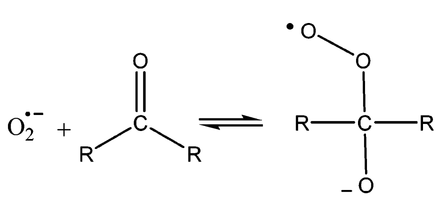

(3)

predicted the existence of an intramolecular nucleophilic addition of the superoxyl O to the carbonyl C, as shown in Figure 7 for EMPO-O_2 *cis*-3B, which is also the most preferred isomer with an exoergicity of −7.0 kcal/mol relative to the least preferred isomer, EMPO-O_2 *cis*-1A. Examination of the optimized geometry of EMPO-O_2 *cis*-3B indicates a conversion of an sp^2-hybridized carbonyl C to sp^3, as indicated by the small $\angle C-C(=O)-O$ angle of 104.7°, the relatively short bond distance between the superoxyl O and the carbonyl C of 1.62 Å, and the elongated C(O)−OEt bond distance of 1.48 Å compared to the average C(O)−OR bond distance of 1.35 Å.

The most favored isomer, DEPMPO-O_2 *cis*-1B (Figure 8), exhibited a unique C−H- - -O interaction with a H- - -O distance of 2.02 Å, which is significantly shorter than the van der Waals radius of 3.30 Å. This C−H- - -O interaction was also predicted for CPCOMPO *trans*-B with an H- - -O distance of 1.98 Å, CPPO-B (2.21 Å), AMPO *trans*-B (2.08 Å), EMPO *cis*-2A (2.14 Å), EMPO *cis*-1B (2.09 Å), DEPMPO *cis*-1B (2.02 Å), and TAMPO *trans*-B (1.98 Å). The C−H- - -O bonding motif has been reported in DNA with an average distance of 2.60 Å, which could contribute to the stability of the macromolecule.[54]

TABLE 7: NPA Spin Densities (Populations) for Selected Superoxide Adduct Structures at the B3LYP/6-31+G//B3LYP/6-31G* Level**

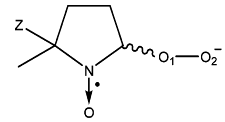

spin adduct	spin density N	O	O_1	O_2
HMPO A[a]	0.262	0.445	0.101	0.204
HMPO B[a]	0.432	0.469	0.057	0.030
DMPO A	0.281	0.445	0.102	0.186
DMPO B	0.466	0.488	0.034	0.001
CPPO A	0.283	0.468	0.092	0.170
CPPO B	0.477	0.477	0.030	−0.001
AMPO *cis*-1A[b]	0.429	0.515	0.031	−0.002
AMPO *cis*-3B[b]	0.432	0.500	0.023	0.002
AMPO *cis*-1B[b]	0.238	0.274	0.169	0.344
AMPO *cis*-1C	0.426	0.522	0.039	0.003
AMPO *cis*-2B[b]	0.406	0.493	0.044	0.059
AMPO *trans*-A	0.212	0.303	0.151	0.351
AMPO *trans*-B	0.481	0.454	0.041	0.009
MAMPO *cis*-H[b]	0.444	0.507	0.019	0.001
MAMPO cis	0.376	0.473	0.078	0.075
EMPO *cis*-1A	0.285	0.491	0.089	0.141
EMPO *cis*-2A	0.281	0.474	0.098	0.169
EMPO *cis*-1B	0.383	0.502	0.048	0.067
EMPO *cis*-2B	0.372	0.488	0.062	0.093
EMPO *cis*-3B[c]	0.400	0.517	0.038	0.002
EMPO *trans*-1A	0.233	0.431	0.105	0.239
EMPO *trans*-1B	0.390	0.465	0.060	0.100
EMPO *trans*-2B[d]	0.453	0.505	0.031	−0.000
DEPMPO *cis*-1A	0.321	0.434	0.103	0.155
DEPMPO *cis*-2A	0.273	0.392	0.117	0.227
DEPMPO*cis*-3A	0.287	0.443	0.099	0.180
DEPMPO *trans*-1A	0.223	0.372	0.131	0.290
DEPMPO *trans*-2A	0.210	0.382	0.121	0.301
DEPMPO *trans*-3A	0.200	0.362	0.128	0.325
DEPMPO *cis*-1B[e]	0.463	0.495	0.010	0.009
DEPMPO *cis*-2B	0.361	0.458	0.063	0.120
DEPMPO *trans*-1B	0.337	0.396	0.099	0.179
DEPMPO *trans*-2B	0.324	0.407	0.097	0.184
DEPMPO *trans*-3B	0.306	0.375	0.115	0.219

[a] A and B denote that the O−O vector is pointing in the same direction as and opposite to N−O, respectively. [b] Involves intramolecular H-bonding: AMPO−O_2 *cis*-1A and AMPO−O_2 *cis*-3B have N−H- - -O_2−O_1, AMPO−O_2 *cis*-1B has N−H- - -O−N, and AMPO−O_2 *cis*-2B has N−H- - -O_1−O_2 bonding mode. MAMPO cis has a CON-(CH_3)H- - -O−O distance of 1.45 Å. [c] With a O−O- - -C═O interaction distance of 1.63 Å. [d] With a C−H- - -O−O interaction distance of 2.14 Å. [e] With a C−H- - -O−O interaction distance of 2.02 Å.

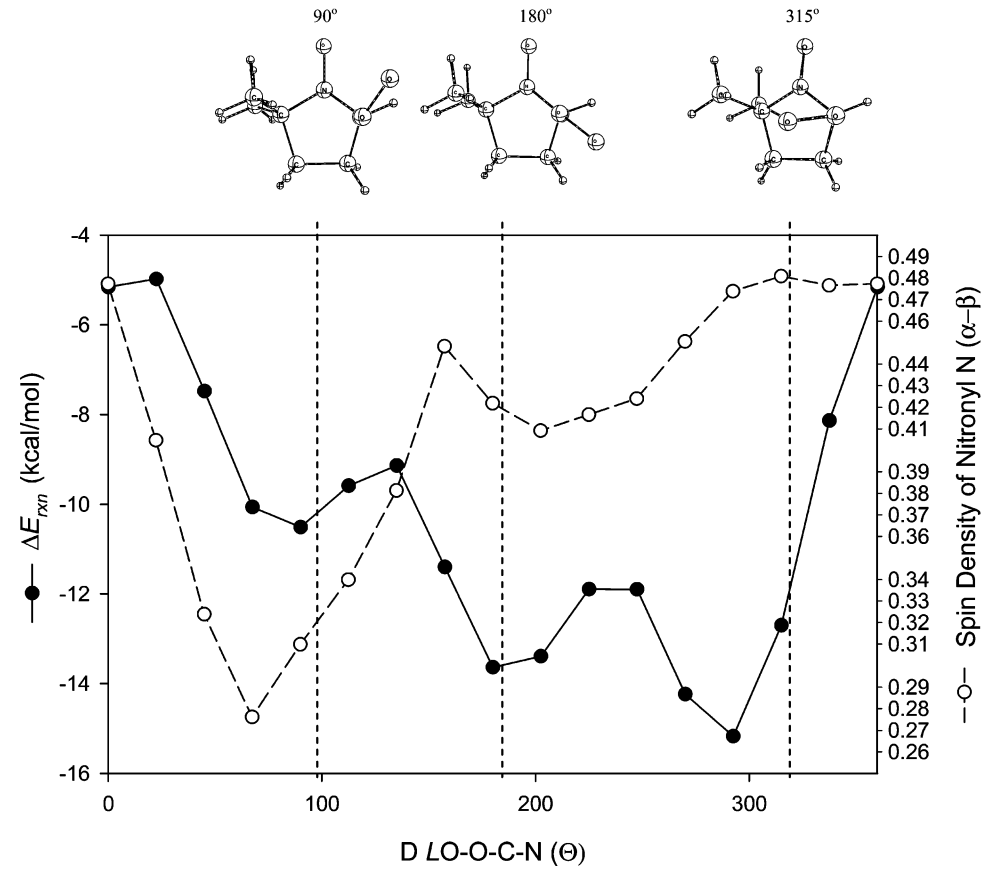

Figure 6. Plots of the bottom-of-the-well reaction energies $\Delta E_{0,\mathrm{rxn}}$ of $O_2^{\bullet -}$ with DMPO at the B3LYP/6-31+G(d,p)//B3LYP/6-31G(d) level and spin densities of the nitronyl N versus the ∠O−O−C−N dihedral angle at 22.5° increments of the DMPO-O_2 adduct.

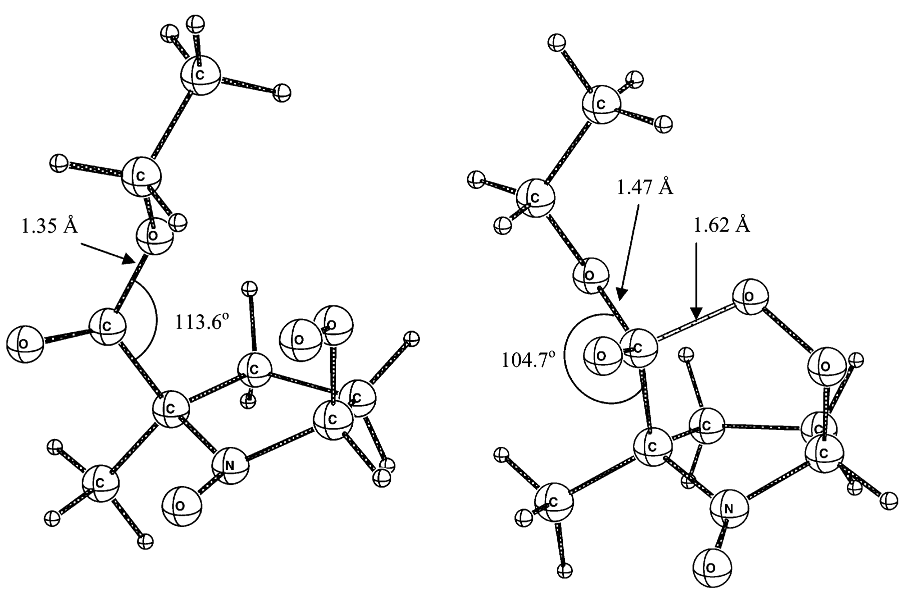

EMPO-O_2 cis-1A
Rel ΔG_{rxn} = 0.0 kcal/mol

EMPO-O_2 cis-3B
Rel ΔG_{rxn} = -7.0 kcal/mol

Figure 7. Views of the B3LYP/6-31G(d) optimized geometry of EMPO-O_2 *cis*-1A (left) and EMPO-O_2 *cis*-3B (right), showing the presence of intramolecular nucleophilic addition to the carbonyl carbon of the ester moiety for the most preferred isomer, EMPO-O_2 *cis*-3B.

Some of the predicted AMPO-O_2 adducts showed intramolecular H-atom transfer reactions from the amide group to the superoxyl moiety (Figure 9). Interestingly, formation of the cis isomers, i.e., AMPO-O_2 *cis*-1A and *cis*-3B, which involves intramolecular H-atom transfer of the amide H to the superoxide unit, is significantly more favorable than the formation of the trans isomers (AMPO-O_2 trans) or cis isomers (AMPO-O_2 *cis*-1B and *cis*-2B; i.e., the superoxide moiety is pointing in the opposite direction from the N−O group) in the absence of such H-atom transfer by about 14 kcal/mol. However, the optimized structure of AMPO-O_2 *cis*-1C, in which the two N−H bonds of the amide group have been restricted and in which the terminal O of the superoxide moiety is closest to the amide H, is less exoergic by 4 kcal/mol than AMPO-O_2 *cis*-1A and *cis*-

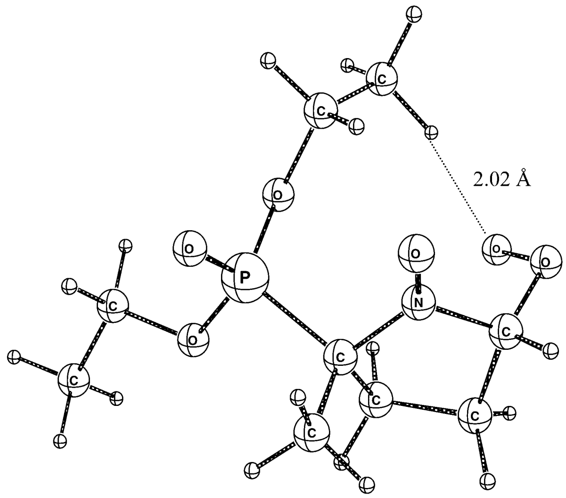

DEPMPO-O_2 cis-1B
ΔG_{rxn} = -1.9 kcal/mol
(relative to the least preferred isomer)

Figure 8. View of the B3LYP/6-31G(d) optimized geometry of the most preferred isomer DEPMPO-O_2 *cis*-1B, showing the presence of an intramolecular C−H- - -O interaction.

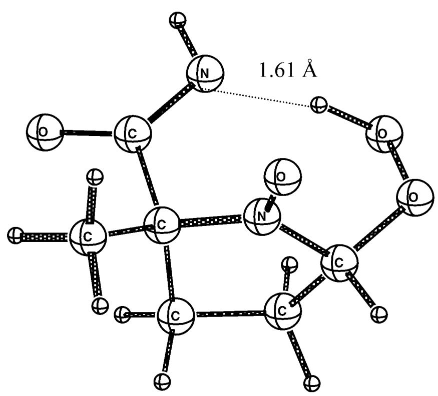

AMPO-O_2 cis-3B
ΔG_{rxn} = -14.9 kcal/mol
(relative to the least preferred isomer)

Figure 9. View of the B3LYP/6-31G(d) optimized geometry of the most preferred isomer, AMPO-O_2 *cis*-3B, showing the presence of the intramolecular H-atom transfer reaction.

3B. We approximate that the free energy for the H-atom transfer reaction is about 4 kcal/mol. The formation of a hydroperoxyl (R−OOH) adduct through H-atom transfer from the amide moiety is described by the formation of O−O- - -H bond and with a bond distance of 1.04 Å and the change in hybridization of the amide N from sp^3 to sp^2. This change in hybridization is characterized by a smaller O═C−N−H dihedral angle of 0.8° and higher C−N−H angle of 114° compared to the amide O═C−N−H dihedral angle of 19.4° and C−N−H angle of 118° for the amide. The intramolecular H-transfer may involve H-atom abstraction rather than proton abstraction, since the pK_a of amides is on the order of 25[55] while that of hydroperoxides (ROOH) is ∼10.[56] Table 7 shows the spin densities on the nitronyl N and O as well as on the two oxygen atoms of the superoxide moiety. It is interesting to note that, in general, the spin density on the terminal superoxide O is significantly high, i.e., from 10 to 35%, in all adducts with **A** projection (θ = 60−70°). This prediction suggests that, upon $O_2^{\bullet-}$ addition to nitrones, the unpaired electron may not completely delocalize to the N−O moiety, as is observed for the $^{\bullet}$OH addition to

TABLE 8: Calculated Relative Enthalpies ΔH^{298K} and Free Energies ΔG^{298K} (kcal/mol) in the Gas Phase and Aqueous Phase (in Parentheses) and Other Theoretical Parameters for the Transition-State Structures of NO Adducts at the B3LYP/6-31+G(d,p)//B3LYP/6-31G(d) Level

structure	$\Delta H^{298K\ d}$	$\Delta G^{298K\ d}$	C- - -N−O (Å)	$\langle S^2\rangle^e$	$N_{imag}{}^f$
		AMPO			
AMPO + NO[a]	0.0 (0.0)	0.0 (0.0)	∞	0.00	0
AMPO-NO[b]	0.1 (1.7)	8.1 (9.7)	2.84	0.75	0
AMPO-NO TS[c]	8.5 (7.3)	19.2 (18.0)	1.83	0.83	1
AMPO-NO	6.1 (3.8)	16.3 (14.0)	1.55	0.92	0
		DEPMPO			
DEPMPO + NO	0.0 (0.0)	0.0 (0.0)	∞	0.00	0
DEPMPO-NO	−0.6 (2.9)	8.5 (12.0)	2.77	0.75	0
DEPMPO-NO TS	6.7 (7.4)	18.4 (19.1)	1.84	0.81	1
DEPMPO-NO	3.9 (4.5)	15.0 (15.6)	1.55	0.92	0
		DMPO			
DMPO + NO	0.0 (0.0)	0.0 (0.0)	∞	0.00	0
DMPO-NO	−0.5 (1.3)	7.8 (9.7)	2.74	0.75	0
DMPO-NO TS	7.0 (4.4)	18.0 (15.3)	1.82	0.82	1
DMPO-NO	4.6 (2.3)	15.1 (12.7)	1.55	0.92	0
		EMPO			
EMPO + NO	0.0 (0.0)	0.0 (0.0)	∞	0.00	0
EMPO-NO	−0.8 (0.8)	7.6 (9.2)	2.74	0.75	0
EMPO-NO TS	6.5 (5.3)	17.7 (16.6)	1.83	0.82	1
EMPO-NO	3.8 (2.5)	14.2 (12.9)	1.55	0.92	0
		CPCOMPO			
CPCOMPO + NO	0.0 (0.0)	0.0 (0.0)	∞	0.00	0
CPCOMPO-NO	−0.4 (1.5)	7.9 (9.9)	2.77	0.75	0
CPCOMPO-NO TS	9.7 (9.6)	20.3 (20.3)	1.92	0.87	1
CPCOMPO-NO	5.3 (4.2)	15.6 (14.5)	1.54	0.79	0

[a] At infinite separation. [b] Nitrone−NO complex. [c] TS stands for transition state. [d] Values in parentheses are relative energies based on single-point energy calculations with the polarizable continuum model (PCM) at the B3LYP/6-31+G** level using water as a solvent. Thermal and entropic corrections from the gas-phase calculations were applied with the single-point energy for the PCM level in order to get estimated ΔH^{298K} and ΔG^{298K} values in water. [e] The $\langle S^2\rangle$ value for all the nitrones is 0.00, while that for NO is 0.75. [f] The point group for all structures is C_1, and N_{imag} refers to the number of imaginary vibrational frequencies (1 = TS). See Figure 10 for a sample schematic representation of the free energies and Table S22 of the Supporting Information for the bottom-of-the-well energies.

nitrones.[15] Although an accurate picture of the mechanism for the H-atom transfer is not clear at the moment, the high spin density (∼34%) on the superoxide O in the AMPO-O_2 adduct could be sufficient to undergo nucleophilic addition to the carbonyl C and subsequent H-atom transfer, as previously shown by the reaction of $O_2^{\bullet-}$ with ethionamide and various thioamides.[57] Hydrogen-atom abstraction by peroxyl radicals (ROO$^{\bullet}$) is also common in lipid peroxidation processes,[50] and it has been reported that the homolytic bond dissociation energies for amide N−H[58] and aliphatic C−H[55,56] bonds are comparable: i.e., 107.5 and 104 kcal/mol. This intramolecular H-atom transfer reaction could be a significant factor for the favorable formation of the cis adduct. Furthermore, the H-atom transfer reaction was only predicted for AMPO but not for MAMPO-O_2 with a

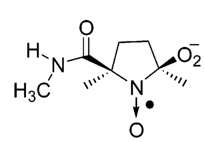

MAMPO-O_2

−C(O)NHCH$_3$ moiety. The MAMPO-O_2 adduct only exhibited intramolecular H-bonding (N−H- - -O) with a distance of 1.45

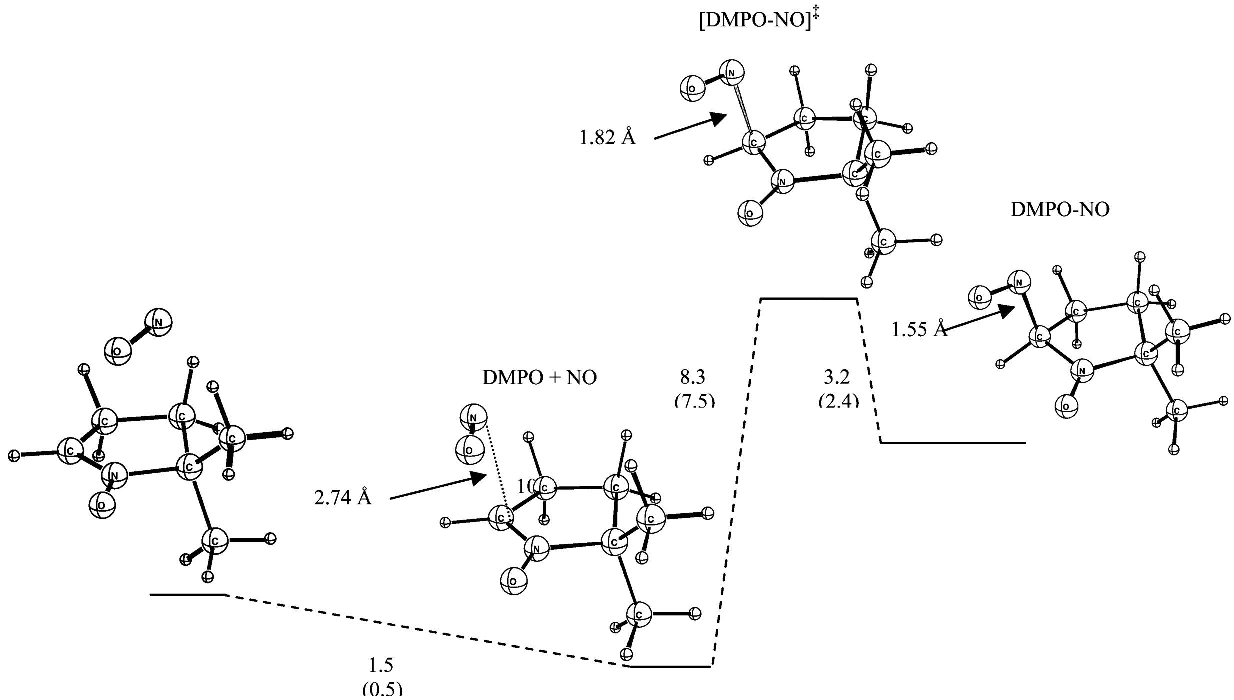

Figure 10. Representative schematic diagram of a typical nitrone reaction with NO in the gas phase (shown for the DMPO-NO reaction), including the transition state [DMPO-NO]‡ for the NO adduct formation. The values are bottom-of-the-well (ΔE) energies (kcal/mol), while the energies in parentheses are enthalpies of reactions (ΔH^{298K}) in kcal/mol obtained at the B3LYP/6-31+G(d,p)//B3LYP/6-31G(d) level. See Tables 8 and S20 for a complete list of energies.

Å and is more favored by about 22 kcal/mol compared to its isomer without intramolecular H-bonding. This preference for the intramolecular H-bonding was also confirmed in the aqueous phase but with only a 14 kcal/mol free energy difference between the formation of the MAMPO-O_2 adduct with and without intramolecular H-bonding.

Hence, in most cases, the most stable $O_2^{\bullet-}$ adduct conformer exhibits intramolecular C−H- - -O H-bonding, except for EMPO and AMPO $O_2^{\bullet-}$ adducts, in which the most stable conformers are those that exhibit intramolecular O═C- - -O−O (via nucleophilic addition) and N−H- - -O−O (via H-atom transfer) interactions which were predicted in EMPO-O_2 *cis*-3B and AMPO-O_2 *cis*-1A (or *cis*-3B), respectively. The optimization of MSMPO-O_2 adducts failed, however.

The thermodynamics of $O_2^{\bullet-}$ addition to nitrones was predicted, and the order of decreasing ΔG_{rxn} (kcal/mol) is as follows: AMPO-O_2 *cis*-3B (−21.1) > AMPO-O_2 *cis*-1C (−16.8) > TFMPO-O_2 *trans*-B (−11.4) > CPCOMPO-O_2 *trans*-B (−11.1) > DEPMPO-O_2 *cis*-1B (−10.8) > TAMPO-O_2 *trans*-B (−9.1) > EMPO-O_2 *cis*-3B (−8.5) > EMPO *trans*-2B (−7.7) > HMPO-O_2 B (−3.7) > DMPO-O_2 B (−3.4) > CPPO-O_2 B (−2.8). Therefore, the order of decreasing stabilization due to intramolecular interaction is H-atom transfer > C−H- - -O H-bonding > nucleophilic addition. These modes of intramolecular interactions and reactions as stabilizing factors could be advantageous and should be taken into consideration in the future design of spin traps with spin adducts with longer half-lives.

Although the average ΔG_{rxn} for the addition of $O_2^{\bullet-}$ to nitrones in water was predicted to be endoergic (9.95 ± 3.04 kcal/mol) compared to the exoergic average ΔG_{rxn} in the gas phase of −7.51 ± 3.67 kcal/mol (Table 2), the qualitative trend of the order of addition of $O_2^{\bullet-}$ to various nitrones remains the same as in the gas phase. However, the influence of various intramolecular interactions on the stability of DEPMPO-O_2 *cis*-1B and EMPO-O_2 *cis*-3B as observed in the gas phase became insignificant in the aqueous phase, while formation of AMPO-O_2 *cis*-3B and AMPO-O_2 *cis*-1C are the most exoergic processes compared to all nitrones that were investigated, similar to that predicted in the gas phase (Table S5). The spin trapping characteristics of AMPO have recently been confirmed experimentally.[48]

Nitric Oxide. The spin density distribution on NO alone shows that 70% of the electron is localized on the N and 30% on the O. At the B3LYP level, the spin densities on the nitroso (N═O) moiety are reduced in all of the NO adducts to an average of 4−11% on the N and 1−7% on the O, while the nitroxyl group N−O has average spin densities of 37% on the N and 50% on the O. The spin density distribution on the N−O of the NO adducts of cyclic nitrones are significantly different compared to the previously reported[43] spin densities on the nitroxyl group of the NO adducts of HNO (N, 13%; O, 75%) and CH_3NO, (N, 13%; O, 74%) using Mulliken population analysis at the HF/6-31G(d) optimized geometry. Optimized structures of most NO adducts gave significant deviation of the average $\langle S^2 \rangle$ values up to 0.92 (see Table 8), except for the CPCOMPO-NO adduct, which had a reasonable $\langle S^2 \rangle$ value of 0.79.

The NO addition to nitrones is disfavored for both enthalpic and free energy reasons, with ΔH_{rxn} = 4−6 kcal/mol and ΔG_{rxn} = 14−16 kcal/mol at 298 K (Table 1), and this is within the order of magnitude predicted for the reaction of NO with nitroso compounds HN═O and CH_3N═O of ΔE_{MP2} = 7.8 kcal/mol at the MP2/6-31G(d,p)//HF/6-31G(d) level of theory.[43] This predicted nonspontaneity of NO addition to nitrones is not surprising since experimental evidence shows that nitrones are not known to trap NO under normal conditions.[41,42] Optimization of the starting structure with a configuration similar to that of **D** only yielded structures with more than one imaginary vibrational frequency. We therefore focused our study of the NO adducts with a conformation similar to that of **C**, and the

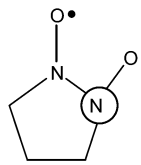

C

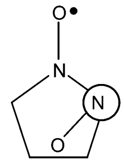

D

corresponding transition state structures for NO addition to the nitrone were also obtained.

Table 8 and Figure 10 shows the free energies and enthalpies of the transition state structures as well as the products for the representative spin traps. At 298 K, the addition of NO to these nitrones has a free energy of activation barrier of 25−28 kcal/mol. To confirm if the energy profile of the NO addition to DMPO shown in Figure 10 will be similar in the aqueous phase, single-point energy calculations with the polarizable continuum model (PCM)[24−28] at the B3LYP/6-31+G** level using water as a solvent were performed. Although the overall energy profile for the formation of DMPO-NO in water as well as in the gas phase are similar, the forward enthalpy of activation is reduced in energy in water as compared to the gas phase, i.e., $\Delta H^{\ddagger}$(289 K,aq) = 4.4 kcal/mol and $\Delta H^{\ddagger}$(289 K,gas) = 7.5 kcal/mol, with an overall reaction enthalpy of ΔH_{rxn}(289 K,aq) = 2.3 kcal/mol and ΔH_{rxn}(289 K,gas) = 4.6 kcal/mol.

The order of increasing endoergicity of NO addition to nitrones is as follows: DEPMPO-NO *trans*-3 (12.0) < MSMPO-NO trans (12.9) < EMPO-NO *trans*-1 (13.5) < HMPO-NO (14.8) < CPPO−NO trans (14.8) < DMPO-NO (15.1) < TFMPO-NO (15.3) < TAMPO-NO trans (15.6) = CPCOMPO-NO trans (15.6) < AMPO-NO *trans*-2 (16.2). The same qualitative trend was predicted in the aqueous phase, in which the formation of NO trans isomers of DEPMPO, MSMPO, and EMPO are the most favored compared to the trans NO adducts of TAMPO, CPCOMPO, and AMPO (Table S6). The average ΔG_{rxn} for the addition of NO to nitrones in water was predicted to be endoergic (14.12 ± 0.93 kcal/mol), similar to the average ΔG_{rxn} in the gas phase of 14.57 ± 1.35 kcal/mol (Table 2).

V. Conclusion

The order of increasing favorability of radical reaction with nitrones is NO < $O_2^{\bullet -}$ < $^{\bullet}O_2H$ < $^{\bullet}SH$ < $^{\bullet}CH_3$ < $^{\bullet}OH$ based on ΔG calculations. A similar trend was predicted in the aqueous phase with only small perturbations computed for the free energies of addition of $^{\bullet}CH_3$, $^{\bullet}SH$, NO, and $^{\bullet}OH$ to various nitrones, while significant changes in free energies were predicted for formation of the $^{\bullet}O_2H$ and $O_2^{\bullet -}$ adducts. In general, the predicted order of increasing favorability for the addition of various radicals to nitrones is largely consistent with their order of increasing reduction potentials and second-order experimental kinetic rate constants. This theoretical approach may be useful in predicting the relative reactivity of other radicals with nitrones. We have shown how intramolecular interactions can govern the favorability of formation of certain adducts in the gas phase. Dominant among these effects are intramolecular H-bonding interactions from −OOH, −SH, and $-OO^-$ moeties. The superoxide adduct of EMPO has been predicted to undergo intramolecular nucleophilic addition of $-O_2^-$ to the carbonyl C in the gas phase but is not thermodynamically favored in the aqueous phase. The presence of a −C−H- - -O−O− interaction has been seen in most of the superoxide adducts, characteristic of the C−H- - -O bonding observed to stabilize macromolecules such as DNA. For $O_2^{\bullet -}$ adduct formation in the gas phase, the order of decreasing stabilization due to intramolecular interaction is H-atom transfer > C−H- - -O H-bonding > nucleophilic addition, where the H-atom transfer mechanism is also the most favored in the aqueous phase. The spin density (population) distribution on the nitronyl N of the $O_2^{\bullet -}$ adducts is dependent on the conformation of the O_2 moiety relative to N−O. The inertness of nitrones toward NO can be ascribed to the endoergic reaction parameters, although transition states in both the aqueous and gas phases could be obtained for NO addition to the nitrones studied here.

Acknowledgment. We wish to thank The Ohio Supercomputer Center (OSC) for support of this research. This work was supported by NIH grants HL38324, HL63744, and HL65608. C.M.H. acknowledges support from the NSF-funded Environmental Molecular Science Institute (Grant No. CHE-0089147).

Supporting Information Available: Tables giving energies, enthalpies, and free energies for all spin traps and their corresponding spin adducts. This material is available free of charge via the Internet at http://pubs.acs.org.

References and Notes

(1) Bilenko, M. V. *Ischemia and Reperfusion of Various Organs: Injury, Mechanisms, Methods of Prevention and Treatment*; Nova Science: Huntington, NY, 2001.
(2) Halliwell, B.; Gutteridge, J. M. C. *Free Radicals in Biology and Medicine*; Oxford University Press: Oxford, U.K., 1999.
(3) Zweier, J. L.; Villamena, F. V. In *Oxidative Stress and Cardiac Failure*; Kukin, M. L., Fuster, V., Eds.; Futura Publishing: Armonk, NY, 2003; pp 67−95.
(4) Augusto, O.; Du Plessis, L. R.; Weingrill, C. L. *Biochem. Biophys. Res. Commun.* **1985**, *126*, 853−858.
(5) Ozawa, T.; Hanaki, A. *Biochem. Intl.* **1990**, *20*, 649−657.
(6) Xia, Y.; Zweier, J. L. *Proc. Natl. Acad. Sci. U.S.A.* **1997**, *94*, 6954−6958.
(7) Richter-Addo, G. B.; Legzdins, P.; Burstyn, J. *Chem. Rev.* **2002**, *102*, 857−860.
(8) Roubaud, V.; Sankarapandi, S.; Kuppusamy, P.; Tordo, P.; Zweier, J. L. *Anal. Biochem.* **1998**, *257*, 210−217.
(9) Giulivi, C.; Poderoso, J. J.; Boveris, A. *J. Biol. Chem.* **1998**, *273*, 11038−11043.
(10) Zhang, H.; Joseph, J.; Vasquez-Vivar, J.; Karoui, H.; Nsanzumuhire, C.; Martasek, P.; Tordo, P.; Kalyanaraman, B. *FEBS Lett.* **2000**, *473*, 58−62.
(11) Olive, G.; Mercier, A.; Le Moigne, F.; Rockenbauer, A.; Tordo, P. *Free Radicals Biol. Med.* **2000**, *28*, 403−408.
(12) Villamena, F. A.; Zweier, J. L. *J. Chem. Soc., Perkin Trans. 2* **2002**, 1340−1344.
(13) Zhao, H.; Joseph, J.; Zhang, H.; Karoui, H.; Kalyanaraman, B. *Free Radicals Biol. Med.* **2001**, *31*, 599−606.
(14) Frejaville, C.; Karoui, H.; Tuccio, B.; Le Moigne, F.; Culcasi, M.; Pietri, S.; Lauricella, R.; Tordo, P. *J. Med. Chem.* **1995**, *38*, 258−265.
(15) Villamena, F. A.; Hadad, C. M.; Zweier, J. L. *J. Phys. Chem. A* **2003**, *107*, 4407−4414.
(16) Villamena, F. A.; Hadad, C. M.; Zweier, J. L. *J. Am. Chem. Soc.* **2004**, *126*, 1816−1829.
(17) Boyd, S. L.; Boyd, R. J. *J. Phys. Chem.* **1994**, *98*, 11705−11713.
(18) Labanowski, J. W.; Andzelm, J. *Density Functional Methods in Chemistry*; Springer: New York, 1991.
(19) Parr, R. G.; Yang, W. *Density Functional Theory in Atoms and Molecules*; Oxford University Press: New York, 1989.
(20) Becke, A. D. *Phys. Rev.* **1988**, *38*, 3098−3100.
(21) Lee, C.; Yang, W.; Parr, R. G. *Phys. Rev. B* **1988**, *37*, 785−789.
(22) Becke, A. D. *J. Chem. Phys.* **1993**, *98*, 1372.
(23) Hehre, W. J.; Radom, L.; Schleyer, P. V.; Pople, J. A. *Ab Initio Molecular Orbital Theory*; Wiley: New York, 1986.
(24) Tomasi, J.; Persico, M. *Chem. Rev.* **1994**, *94*, 2027.
(25) Cossi, M.; Barone, V.; Cammi, R.; Tomasi, J. *Chem. Phys. Lett.* **1996**, *255*, 327.
(26) Barone, V.; Cossi, M.; Tomasi, J. *J. Chem. Phys.* **1997**, *107.*, 3210.
(27) Barone, V.; Cossi, M.; Tomasi, J. *J. Comput. Chem.* **1998**, *19*, 404.
(28) Cossi, M.; Barone, V. *J. Chem. Phys.* **1998**, *109*, 6246.
(29) Frisch, M. J.; Trucks, G. W.; Schlegel, H. B.; Scuseria, G. E.; Robb, M. A.; Cheeseman, J. R.; Zakrzewski, V. G.; Montgomery, J., J. A.; Stratmann, R. E.; Burant, J. C.; Dapprich, S.; Millam, J. M.; Daniels, A. D.; Kudin, K. N.; Strain, M. C.; Farkas, O.; Tomasi, J.; Barone, V.; Cossi, M.; Cammi, R.; Mennucci, B.; Pomelli, C.; Adamo, C.; Clifford, S.;

Ochterski, J.; Petersson, G. A.; Ayala, P. Y.; Cui, Q.; Morokuma, K.; Rega, N.; Salvador, P.; Dannenberg, J. J.; Malick, D. K.; Rabuck, A. D.; Raghavachari, K.; Foresman, J. B.; Cioslowski, J.; Ortiz, J. V.; Baboul, A. G.; Stefanov, B. B.; Liu, G.; Liashenko, A.; Piskorz, P.; Komaromi, I.; Gomperts, R.; Martin, R. L.; Fox, D. J.; Keith, T.; Al-Laham, M. A.; Peng, C. Y.; Nanayakkara, A.; Challacombe, M.; Gill, P. M. W.; Johnson, B.; Chen, W.; Wong, M. W.; Andres, J. L.; Gonzalez, C.; Head-Gordon, M.; Replogle, E. S.; Pople, J. A. *Gaussian 98*; Revision A.11.3; Gaussian, Inc.: Pittsburgh, PA, 2002.

(30) Scott, A. P.; Radom, L. *J. Phys. Chem.* **1996**, *100*, 16502−16513.

(31) Reed, A. E.; Weinhold, F. A.; Curtiss, L. A. *Chem. Rev.* **1998**, *98*, 899.

(32) Gonzales, C.; Schlegel, H. B. *J. Phys. Chem.* **1990**, *94*, 5523.

(33) Gonzales, C.; Schlegel, H. B. *J. Chem. Phys.* **1989**, *90*, 2154.

(34) Arranz Mascarós, P.; Gutiérrez Valero, M. D.; Low, J. N.; Glidewell, C. *Acta Crystallogr.* **2003**, *C59*, o210−o212.

(35) Steiner, T. *Acta Crystallogr.* **2000**, *C56*, 876−877.

(36) Buettner, G. R. *Arch. Biochem. Biophys.* **1993**, *300*, 535−543.

(37) Finkelstein, E.; Rosen, G. M.; Rauckman, E. J. *J. Am. Chem. Soc.* **1980**, *102*, 4995.

(38) Pou, S.; Ramos, C. L.; Gladwell, T.; Renks, E.; Centra, M.; Young, D.; Cohen, M. S.; Rosen, G. M. *Anal. Biochem.* **1994**, *217*, 76−83.

(39) Davies, M. J.; Forni, L. G.; Shuter, S. L. *Chem.-Biol. Interact.* **1987**, *61*, 177−188.

(40) Tsai, P.; Ichikawa, K.; Mailer, C.; Pou, S.; Halpern, H. J.; Robinson, B. H.; Nielsen, R.; Rosen, G. M. *J. Org. Chem.* **2003**, *68*, 7811−7817.

(41) Arroyo, C. M.; Kohno, M. *Free Radical Res. Commun.* **1991**, *14*, 145−155.

(42) Pou, S.; Keaton, L.; Surichamorn, W.; Frigillana, P.; Rosen, G. M. *Biochim. Biophys.* **1994**, *1201*, 118−124.

(43) Boyd, S. L.; Boyd, R. J. *J. Phys. Chem.* **1994**, *98*, 1856−1863.

(44) Silva, C. O.; da Silva, E. C.; Nascimento, M. A. C. *J. Phys. Chem. A* **2000**, *104*, 2402−2409.

(45) Lide, D. R., Ed. *CRC Handbook of Chemistry and Physics*; CRC Press: Boca Raton, FL, 1996.

(46) Allen, F. H.; Bird, C. M.; Rowland, R. S.; Raithby, P. R. *Acta Crystallogr.* **1997**, *B53*, 696−701.

(47) Alini, S.; Citterio, A.; Farina, A.; Fochi, M. C.; Malpezzi, L. *Acta Crystallogr.* **1998**, *C54*, 1000−1003.

(48) Villamena, F. A.; Rockenbauer, A.; Gallucci, J.; Velayutham, M.; Hadad, C. M.; Zweier, J. L. *J. Org. Chem.* **2004**, *69*, 7994−8004.

(49) Filippova, T. M.; Lavrukhin, B. D.; Shmyrev, I. K. *Org. Magn. Reson.* **1974**, *6*, 92−98.

(50) Halliwell, B.; Gutteridge, J. M. C. In *Free Radicals in Biology and Medicine*; Oxford University Press: Oxford, U.K., 1999; pp 60−61.

(51) Gibian, M. J.; Sawyer, D. T.; Ungermann, T.; Tangpoonpholvivat, R.; Morrison, M. M. *J. Am. Chem. Soc.* **1979**, *101*, 640−644.

(52) Sawyer, D. T.; Stamp, J. J.; Menton, K. A. *J. Org. Chem.* **1983**, *48*, 3733−3736.

(53) Johlman, C. L.; White, R. L.; Sawyer, D. T.; Wilkins, C. L. *J. Am. Chem. Soc.* **1983**, *105*, 2091−2092.

(54) Berger, I.; Egli, M.; Rich, A. *Proc. Natl. Acad. Sci. U.S.A.* **1996**, *93*, 12116−12121.

(55) Gordon, A. J.; Ford, R. A., Eds. *The Chemist's Companion: A Handbook of Practical Data, Techniques, and References*; Wiley-Interscience: New York, 1972.

(56) Jonsson, M. *J. Phys. Chem.* **1996**, *100*, 6814−6818.

(57) Paez, O. A.; Valdez, C. M.; Tor, J.-F. *J. Org. Chem.* **1988**, *53*, 2166−2170.

(58) Bordwell, F. G.; Algrim, D. J.; Harrelson, J., J. A. *J. Am. Chem. Soc.* **1988**, *110*, 5903−5904.

(59) Xu, Y. K.; Chen, Z. W.; Sun, J.; Liu, K.; Chen, W.; Shi, W.; Wang, H. M.; Zhang, X. K.; Liu, Y. *J. Org. Chem.* **2002**, *67*, 7624−7630.

(60) Villamena, F. A.; Dickman, M. H.; Crist, D. R. *Inorg. Chem.* **1998**, *37*, 1446−1453.

(61) Boeyens, J. C. A.; Kruger, G. J. *Acta Crystallogr.* **1970**, *B26*, 668.

(62) Roubaud, V.; Siri, D.; Tordo, P.; Hdii, F.; Reboul, J.-P. *Acta Crystallogr. C* **1998**, 825−827.

(63) Puliti, R.; Mattia, C. A.; Lilley, T. H. *Acta Crystallogr.* **1992**, *C48*, 709−712.

(64) Parvez, M.; Clark, P. D.; Primak, A. *Acta Crystallogr.* **2003**, *E59*, o783−o785.

(65) Bats, J. W.; Weyrauch, J. P.; Hashmi, S. K. *Acta Crystallogr.* **2002**, *E58*, o590-o591.

(66) Hossain, M. B.; Van der Helm, D. *Acta Crystallogr.* **1983**, *C39*, 1297−1300.

(67) Dickman, M. H. *Acta Crystallogr.* **2001**, *E57*, o636−0637.

(68) Das, T. N.; Huie, R. E.; Neta, P.; Padmaja, S. A. *J. Phys. Chem., A* **1999**, *103*, 5221−5226.

(69) Bartberger, M. D.; Liu, W.; Ford, E.; Miranda, K. M.; Switzer, C.; Fukuto, J. M.; Farmer, P. J.; Wink, D. A.; Houk, K. N. *Proc. Natl. Acad. Sci. U.S.A.* **2002**, *99*, 10958−10963.